Terrestrial Radar Interferometry Monitoring during a Landslide Emergency 2016, Ghirone, Switzerland

Caduff Rafael, Strozzi Tazio

Abstract

In early spring 2016 an exceptionally high rock-fall activity in a slope above the Village of Ghirone, Blenio-Valley Ticino, Switzerland was observed. Constant rock-fall activity was induced by toppling movement of the very thin-layered metamorphic rock. At this time, there was no information on the actual extent and the deformation rates of the landslide instability. Due to the rock-fall and failure related risk, no instrumentation on-site was possible. Local authorities then decided setting up a monitoring campaign using terrestrial radar interferometry that does not need installations in the target area. A campaign was started in the morning of 22 March 2016. Shortly after the beginning of the measurements, the extent of the active area could be determined, showing a total affected area of 5,300 m^2. The displacement velocity was in the range of 0.02-0.05 m/h, showing an increasing trend. Using inverse velocity extrapolations, a failure forecast could be done pointing to a potential failure event in the late afternoon of the same day. At 16:45 UTC+1 a major part of the slope failed. It was only 1/3 of the expected volume. Landslide activity continued and a second major failure was recorded in the night. The emergency campaign ended on 24 March 2016 after the deformation was decreasing to a level without imminent threat to the village. A refined post-processing of the radar data showed that the simplified real-time processing approach was suitable for the situation. Additionally, information on the 2d direction of the landslide movement could be obtained using intensity image pixel tracking technique. Finally, maps of volume differences could be created using the interferometric baseline, showing a difference of 33,900 m^3 between 22 March and a later campaign performed on 31 May 2016.

Keywords

terrestrial radar interferometry, landslide, toppling, failure forecast, real time monitoring

Introduction

Even though a depiction of a general trend in increasing landslide activity is difficult, a statistical analysis of landslide events in the European Alps showed that spring and early summer show an increased seasonal activity (Wood et al., 2016). In most cases of sudden landslide events in previously stable slopes, there is lack of monitoring data giving quantitative information on the displacements and the actual displacement velocity. On-site installation of reference targets and other measurement installations are often hindered by increased rock-fall activity and an increased risk by entering the active landslide area. Therefore, visual inspection from afar and remote sensing techniques such as photogrammetry, laser scanning and radar interferometry are methods used to gain further information that is useful for the hazard and emergency management (Metternicht et al., 2005; Casagli et al., 2010; Jaboyedoff et al., 2012).

Terrestrial radar interferometry offers a quick method for the determination of the velocity field of an active landslide (Tarchi et al., 2003; Casagli et al., 2010; Lowry et al., 2013; Crosta et al., 2014; Caduff et al., 2014). It is used as well to monitor the landslide-activity in a near-real time mode, giving an excellent tool for emergency management. It gives very precise information on the surface displacement without the need for on-site installation and therefore minimizing the risk for the investigation.

Here, we present data of terrestrial radar interferometry of the Ghirone Landslide in the Blenio Valley, Ticino Switzerland. Data was acquired during a 2-day emergency campaign from 22-24 March 2016. In total, 3,036 acquisitions were taken with 1 minute intervals and processed in real time, allowing tracking the line of sight velocity and forecasting failure events.

In this paper, we present the results from the interferometric processing. Additionally, results of the

intensity pixel tracking evaluation are shown. These show the directed 2d displacement of the landslide. Finally, using the vertical interferometric baseline of the upper and lower receiving antenna of the interferometer, we were able to quantify a volume loss of 33,900 m³ in the landslide body over 2 months.

The Ghirone landslide

The Ghirone landslide is located in Blenio Valley, Ticino, Switzerland (Fig. 1a). It lies above the village of Ghirone Aquilesco. The terrain at the village is at an elevation of 1,217 m a.s.l. and climbs up in direction north-east to an elevation of 2,110 m a.s.l. In 1,300 m lateral distance, the secondary summit of Pizzo Pianca is located. From here, several couloirs reach down to the valley bottom and supply debris deposits upon which the village is built on.

A small road is crossing the debris-cone in several serpentines. The road leads to the Lake Luzzone, a major arch-dammed lake that is used for hydro power generation. This road is the only land access to the dam-site. Although the road is mainly used by the local power plant operator, during summer it is frequently used for touristic excursions up to the Lake Luzzone area.

At the summit area, first ground movement was observed end of March 2016 after snow melt by the inhabitants of the village. The ground movement was indicated by an increasingly high rockfall activity.

From the geological point of view, the landslide source area lies in the Bündner-Schist area of the Grava Nappe. The lithology is dominated by calcareous mica schist inter-layered with dark clay schist. The bedding dips in NNE direction with an inclination of 75° and lies more or less normal to the topography creating a counter-dip slope bedding in the metamorphic rocks (Baumer et al., 2013). An inspection of the landslide by geologists revealed that the mechanics of the landslide could be two-folded. First, toppling movement is clearly visible and it is in agreement with the general structural setting. Secondly, sliding movement along a basal gliding plane is possible as well, which is indicated by the almost vertical movement of the terrain along the main scarp (12-15 m high). The grain size of the material is dominated by the very thin layering of the rock, only few larger components are seen in the rock mass. Attention is given in special on the larger boulders that prone to fail, because they hold the potential to reach the lower part of the slope where the road and the village are located.
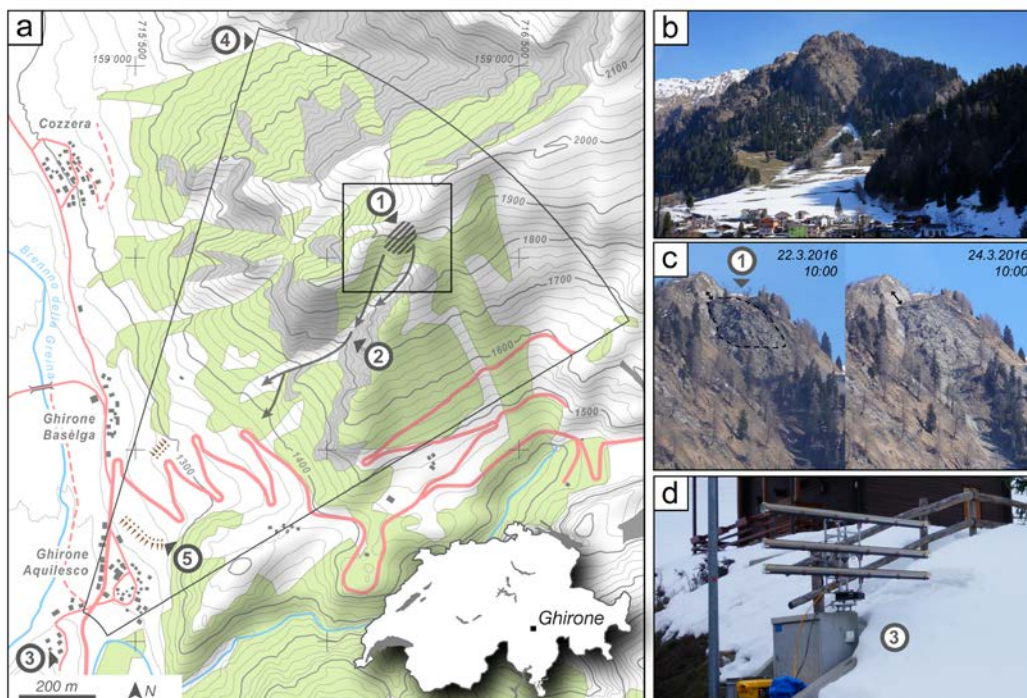
Fig. 1 a: Map overview of the study site. b: target area seen from GPRI location. c: Detail of the landslide area. d: GPRI setup. The site is located in the Blenio Valley, Ticino Switzerland. The Landslide source area (1) is located above the Village of Ghirone Aquilesco. Possible debris paths are indicated in (2). The area is monitored with the Gamma Portable Radar Interferometer (GPRI) that was setup at the valley bottom at location (3). The visible surface within area (4) is covered by the radar acquisitions. After the main failure event, local authorities built a protection dam (5) to prevent mobilized sediment to reach the village.

Measurement setup

The Gamma Portable Radar Interferometer GPRI

The GAMMA Portable radar interferometer (GPRI) (Werner et al. 2012) was deployed shortly after notice of the local authorities. The setup was made on a temporary mounting plate on a local power distribution cabinet. The azimuth tracker motor was fixed on the base plate that remained for potential reposition at a later stage of the observation (Fig. 1d).

The GPRI operates at a frequency of 17.1-17.3 GHz (Ku-Band). The wavelength is therefore 1.74 cm. In each acquisition, the magnitude and phase of the backscattered signal is recorded and forms a 2-dimensional complex-valued image of the area. The image is generated by the physical rotation of the real aperture antennas around the rotation center. In the case of the Ghirone Landslide, a 45° rotation was used to cover the area that is indicated in Fig. 1a. The timing necessary for a single acquisition was 5 sec.

The resolution of the radar image is 75 cm in range and roughly 2.6 m in cross-range at the landslide area (slant range: ~1,500 m). This corresponds to 4-time oversampling with respect to the real antenna aperture of 0.4°. The general working principle and a comprehensive analysis on the general interferometric processing step as applied in the following section are described in more detail in Caduff et al. 2014.

Real Time Data Processing for quick situation evaluation

Due to the time-sensitivity of the assessment, a robust analysis method of the data was used. Since no a-priori information on the potential displacement rates was available, the acquisition rate was set to 1 min^{-1}. This allows an uncritical assessment of a displacement of up to 0.25 m/h which corresponds to the critical wavelength of $\lambda/4$.

However, in general the interferometric phase is disturbed by changes in the atmospheric conditions and random movements within the radar resolution cell. In the case of the landslide, on the one hand, the random movement is invoked by the vegetation cover but as well by the very high rock-fall activity in the landslide source area and the debris-deposit area underneath.

Both, the atmospheric contribution and the random phase, prevent a direct conversion from the calculated phase difference to absolute displacement values. Since the target area is relatively close to the instrument (~1,500 m slant range distance), the non-linear atmospheric contribution is believed to fall below the significance level averaging multiple observations. Similar effect is expected to happen with random phase due to decorrelation events.

Therefore, it was decided to create stacks of observations at 30 min temporal resolution (30 scenes). Stacks were created by calculation of the interferometric phase from the actual acquisition to the previous. The interferometric phase was normalized to a reference point and converted to velocity maps using the wrapped phase as shown in Fig. 2. Due to the nature of the interferometric observations, only displacement in line of sight (LOS) can be measured.

Although, that in general, an unwrapping procedure is applied on the differential interferogram, it was not done in this case. There are several reasons for this decision: the computational effort needed to process the amount of data and the relatively high amount of errors in this process for the very small patches that are above the threshold. In addition, deformation exceeding the 2π can be identified in the field by the operator using a wrapped color cycle for the visualization of the results.

Generated single observation velocity maps were added to the stack. The incomplete stack could always be investigated and the updated information could be extracted. Additionally, the single interferograms and coherence maps were stored as well for the investigation of the timing of possible larger failure events.

Landslide extent and timing of the failure events

After few acquisitions in the field, the extent of the area in motion and the LOS velocity could already be determined. The area of the landslide at this moment was roughly 5,300 m². As it can be seen in Fig. 2, the exposure line of the basal gliding plane cuts the bedrock wedge, that divides the upper part of the mountain in two parts in the middle and not underneath as it was worried. The latter case would have tripled the volume calculations for a potential full failure. With the observed outline, a volume estimation of 80,000 m3 was communicated by the geologists.

The continued measurements showed a slight increase in velocity. After a few more observations, failure forecast using the inverse velocity method (Fukuzono, 1985) was done (Point A in Fig. 3). It showed that a landslide failure was imminent and supposed to take place in the afternoon. Indeed, in the mid-afternoon, starting at around 16:00 UTC+1 an increased fall activity was observed visually and in an increased decorrelation in the 1-minute interferograms. On 16:45 UTC+1 a major failure happened affecting only an estimated third of the total volume that prone to fail. The recorded velocity up to this point was around 0.18 m/h.

After the failure event, the movement decelerated again to levels of ~0.025 m/h. During the night, a second acceleration event was recorded that led again

to a partial failure. However, no visual validation of this event was available.

Following this second major event, the velocity of the landslide was highly variable with some minor failures. The orographic lower right side of the landslide came to a complete stop (point A, Fig. 3). As well point B (Fig. 3) that is located in the center but orographic right side of the landslide showed a strong deceleration in the morning of the third day (24 February 2016). After a velocity of 0.01 m/h was reached, a slight and linear increase of the velocity was recorded again. Fig. 2 shows that the signature of this acceleration was very localized and pointing to the left couloir that is not directly linked with a path towards the village but traverses a depositary region with less inclination. The measurement was stopped at this point, since for the local authorities no imminent threat to the village was present at that time. However, additional measurement campaigns on 12 April 2016 (duration: 8 h) and 31 May–3 June 2016 (duration: 73 h) were taken for control purposes respectively as part of a monitoring concept during a truck convoy that had to climb the road that crosses the transit and deposition zone of the landslide.

Post event data processing: Finding the ideal monitoring approach

Interferometric analysis (1d-Displacement)

In general, the same processing-workflow as for the real-time method that was applied to different settings in the post-processing. The focus was set on the generation of averaged stacks covering different sampling intervals. In addition to the real-time processing, a better selection of reference points that remained stable during the entire duration of the campaigns could be performed. The interferometric phase was normalized to those stable reference points right outside the landslide flanks (Points N1-N3 in Fig. 2).
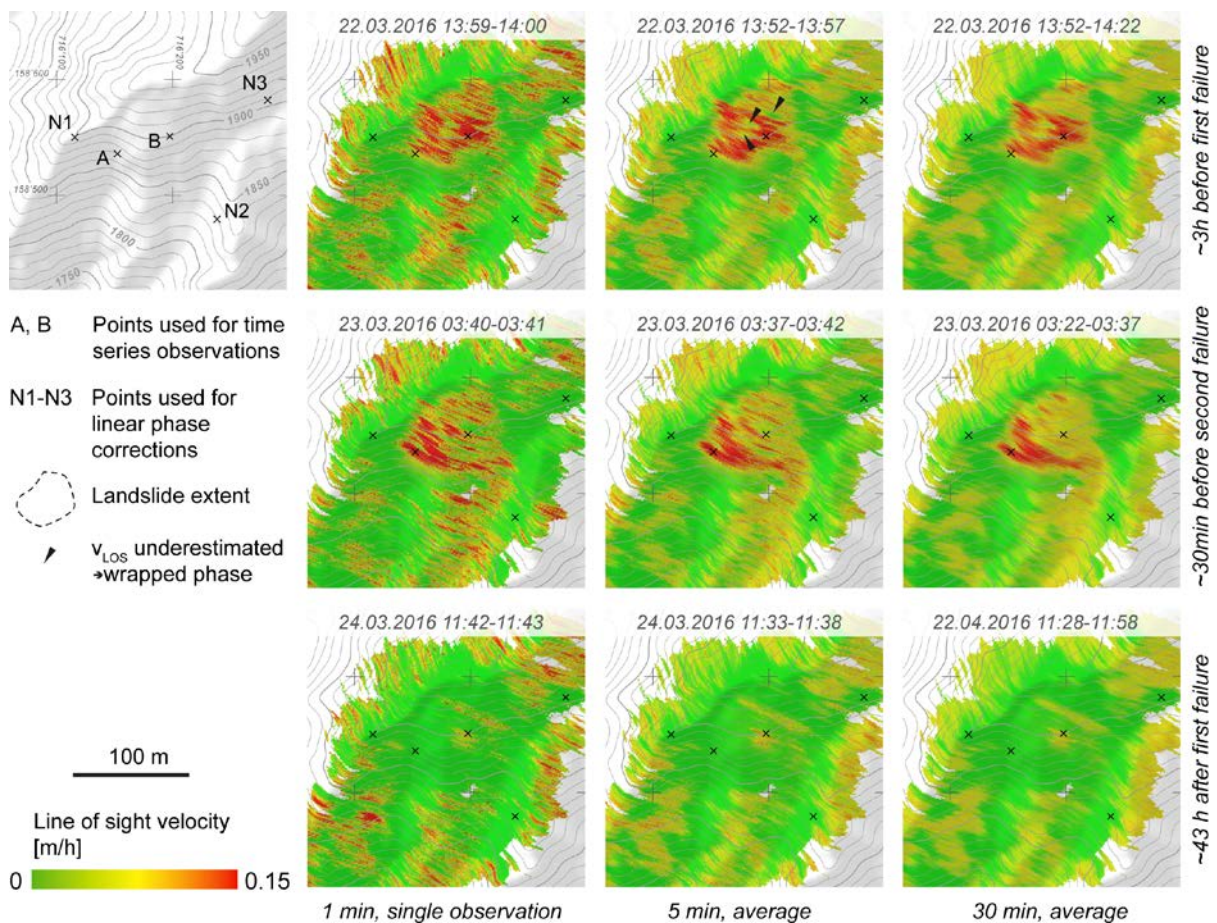
Fig. 2 Line of sight velocity maps taken at different times with different temporal oversampling (averaging).
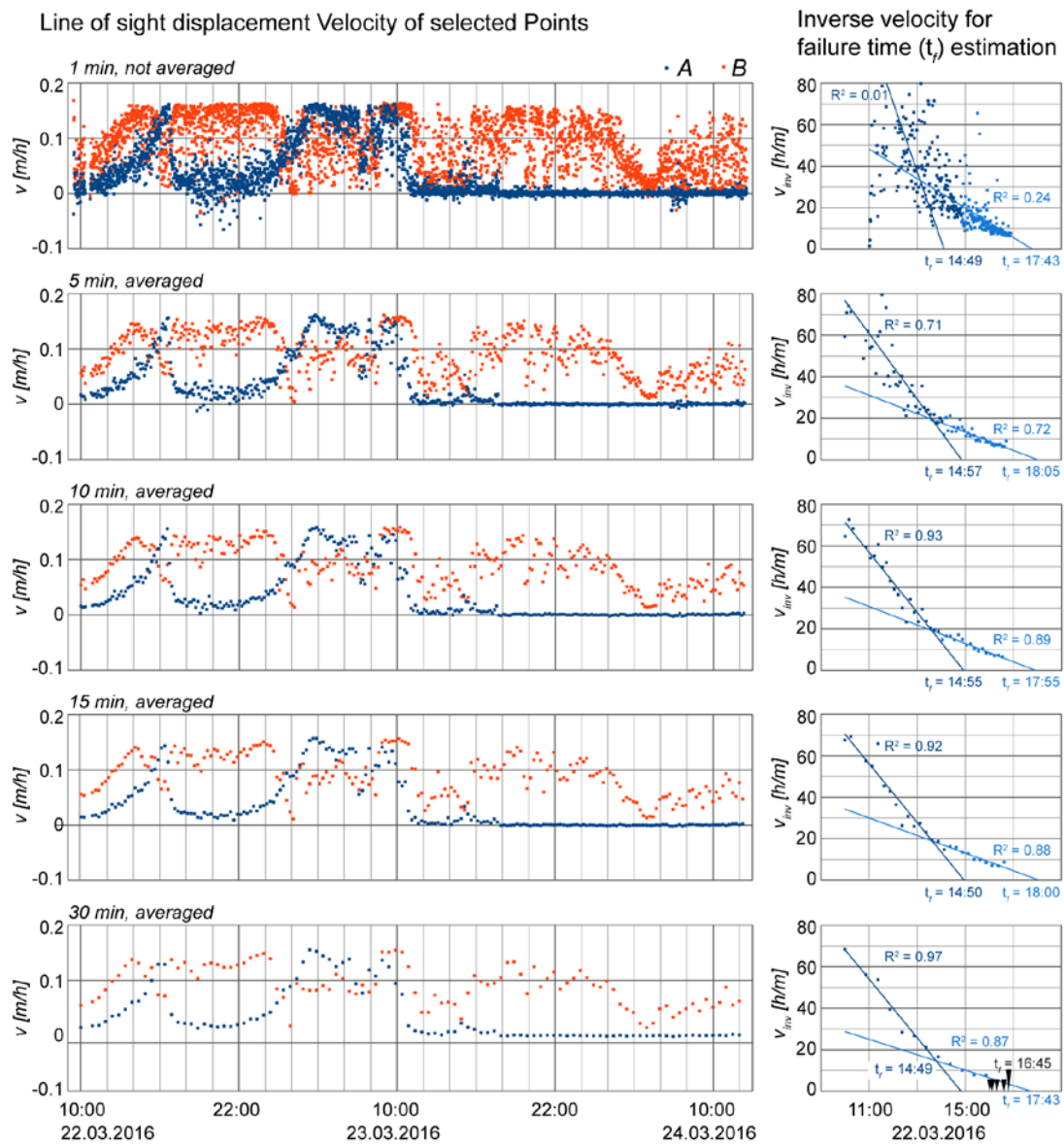
Fig. 3 Time series of the line-of-sight velocities at two selected points (A and B). The location of the points is indicated in the detail map of Fig. 2. On the right side, the inverse velocity (1/v) is shown from beginning of the campaign, until shortly before the first major failure event that took place at 16:45 UTC+1. The black arrows at the bottom diagram show the time of the smaller and the major failure event. The temporal sampling for the velocity time series and the inverse time-series is increased from top to bottom. Values were calculated by stacking of radar acquisitions.

Post-processing method

The first campaign started on 22 March 2016 09:25 UTC+1 and ended on 24 March 2016 12:30 UTC+1. In those 51 hours of measurements where nominal every minute an image was acquired, a total of 3,036 single-

look complex image pairs (upper and lower receiving antenna) was collected.

In the post processing, those scenes were interferometrically processed for a re-assessment of the applied approach during the landslide failure events. Due to the very fast recorded movements in the center

area of the landslide, only 1 minute time-steps were processed. Interferograms were calculated and now wrapped phase values were converted directly to 1d-displacement velocity maps in the unit of m/h. Those maps were then grouped to stacks of 1, 5, 10, 15 and 30 minutes. The velocity maps were then compared for selected times before and after major failure events. In the comparison, it was taken care that the stacks do only cover pre- or post-event scenes and were not mixed.

Post-processing results

The results of the detailed analysis are shown in Fig. 2 and Fig. 3 where a selection of results from the different stacking intervals is shown. The 1 minute velocity maps show slightly more noise and especially within the area under deformation more patches that appear green, meaning slower movement. From a mechanical point of view, this is very unlikely. Those small patches indicated with arrows show local wrapped movement crossing 2π deformation in 1 minute. However, the amount of those patches is reduced with the increasing number of observations indicating as well decorrelation due to local failures and triggered rock-fall in single interferograms. The borders of the landslide tend to sharpen as well with increasing number of scenes in the stack.

The time-series of the deformation in Fig. 3 shows during the entire campaign that several acceleration cycles happen. However by looking at only a very short time period, the values show very high variability. This variability prevents the assessment of the general movement trend. Averaging only 5 observations is enough to draw the general deformation trend that is not significantly enhanced with increasing number of observations. However, a larger number of scenes in the stack reduce the atmospheric phase noise better, when atmospheric conditions are more turbulent.

Intensity pixel tracking (2d-Displacement)

The landslide is affected by relatively large displacement of several meters per day. One example is visible in Fig. 1c. Here, the scarp length at the first day and two days later is marked in the images with a small double arrow. The length of the exposed scarp nearly doubled up to around 15-18 m in this time because of the downward-movement in the landslide.

If the movement is coherent (e.g. "flow-like"), image tracking techniques can be applied to the radar backscatter intensity images. The technique is widely used for glacier flow tracking using space-borne radar imagery (Strozzi et al., 2002). For terrestrial radars in the geo-scientific use, Crosetto et al. (2014) showed an example for a slow landslide, but using artificial corner reflectors installed inside the landslide area that have a

unique radar cross section compared to the surrounding areas.
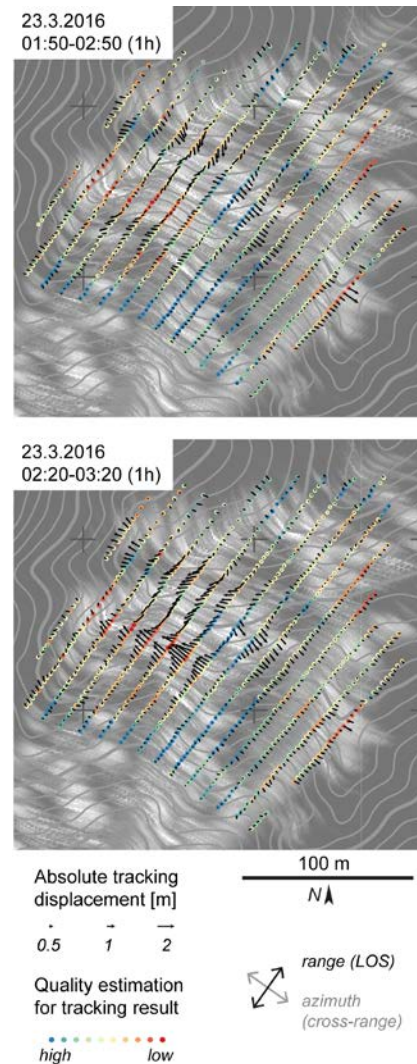
Fig. 4 Tracking results on top of two pairs of backscatter intensity images. The images show the displacement right before the second major failure event that happens at 03:50 UTC+1.

Pixel tracking method

For a quick assessment of the potential of the tracking technique in the Ghirone case, the IMCORR software was used on the scaled backscatter intensity raster (8 bit) images. The used tracking algorithms are discussed in Scambos et al. (1992).

The single observations of the radar backscatter suffer from speckle (noise), especially in areas with dense vegetation cover and on the landslide front, where constant rock-fall activity is observed. Due to

this reason, multiple observations were averaged. For the result in Fig. 4, each image used for the tracking approach consists of 30 averaged scenes that were acquired every minute. As result, the noise in the intensity images could be reduced.

In a second step, pairs were selected and the tracking was executed on the images in slant range geometry. The sample spacing of 5×5 pixels was used and a search window of 64×32 pixels. The resulting point displacements were then geocoded and a rotation of the displacement vectors to the new position was applied. Finally, a conversion of the displacement from pixels to meter was performed.

Pixel tracking results

The result of the processing is shown in Fig. 4. The quality indicator shows that the highest displacements that are directed in cross-range direction are mostly of low quality. This is in agreement with visual findings on the images. This section corresponds to the landslide front and is heavily disturbed by rock-fall and small failure events.

The center of the image shows medium to high quality pixel tracking results. The vectors point toward south-east into the orographic left couloir that leads away from the landslide. The determined 2d-displacement reaches up to 1 m in 1 h, what is in agreement with the interferometrically determined activity at the same time (Fig. 2). Note, that phase jumps in the wrapped phase in this area lead to under-estimation of the actual displacement especially in the center of the landslide (see arrows in Fig. 2). In addition, an under-estimation of the displacement rate is measured, since only the LOS-vector component with regard to the actual pointing of the displacement vector, that is a-priori not known, is measured.

Volumetric change

The landslide and failure activity led to volume changes in the source area. One approach to determine those volume changes is given by calculation using pre- and post-event digital elevation models. A second approach that was applied in this study is shown below. This approach converts phase differences directly to vertical elevation differences.

Volumetry method

For a quick topographic reconstruction we used the approach described in Strozzi et al. (2012), where the vertical baseline of the GPRI is used to calculate elevation information. In our case, a pre-failure scene, taken on 22 March 2016 at the beginning of the first measurement campaigns, was compared to a scene acquired on 31 May 2016. In the processing strategy selected for the Ghirone landslide, we decided to unwrap the difference of the two GPRI single-pass interferograms to directly compute a height difference map. The later was resampled to 1 m posting in rectangular coordinates and the height differences within the landslide regions were summed up to come up with a volume estimate.

Volumetry results

The result of the volumetric change measurement is shown in Fig. 5. Although quite noisy, the area affected by the landslide can be well recognized with the two distinct sectors (see arrows). In addition to the presented elevation change map, the volumetric difference of 33,900 m^3 was calculated for the observed period.
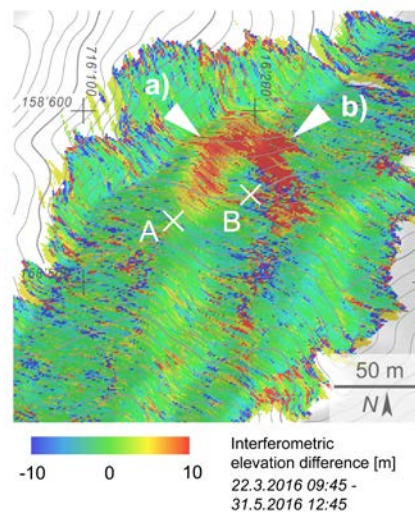
Fig. 5 Result of the height change evaluation using the single pass differential interferograms of the upper and the lower receiving antennas during the presented campaign and 2 months after.

Conclusions

The emergency monitoring using the Gamma Portable Radar interferometer (GPRI) during the Ghirone landslide event took place from 22-24 March 2016. Real time monitoring of a simplified interferometric approach using stacks of wrapped interferograms, converted to LOS-displacement velocity allowed the instantaneous determination of the landslide extent, its temporal characterization and the application of the inverse velocity method led to the forecast of a failure event. The failure happened at the afternoon of the first day and was indicated a few hours before by the measurements within a span of ~3 h. The field data was communicated on a regular basis to the local authorities that used it for the emergency management.

A thorough post-processing of the data showed that the applied simplified approach is indeed very

helpful during very fast (up to 0.25 m/h) processes that are disturbed by decorrelating events such as constant rock-fall and small partial rock-failures.

Image tracking techniques show the potential of giving additional information on the direction of the movement and for cases where the velocity exceeds the critical velocity that is determined by the used wavelength and the repetition interval (0.25 m/h@1 min).

However, due to speckle effects, multiple observations had to be averaged to apply the pixel tracking algorithms successfully. In general, a slight over-estimation and a higher error sensitivity of the deformation in the cross-range direction are observed. This is explained by the roughly 4 times lower resolution at the presented range distance of ~1,500 m.

Finally, the volume difference of 33,900 m^3 between 22 March 2016 and an additional campaign on 31 May 2016 could be determined using the single pass interferograms with a baseline of 25 cm that is given by the upper and lower receiving antennas.

With this campaign, the readiness of terrestrial radar interferometry was shown in the monitoring of exceptional events with difficult conditions. It has shown as well the potential for further developments in the pixel tracking method and in the volume estimation using vertical baseline that might as well be useful at a field-ready level in future cases.

Acknowledgments

References

Baumer A, Egli W, Frey J D, Jung W, Riemann A, Uhr A, Vögeli S, Wiederkehr M (2013) Sheet 1233 Greina. - Geological Atlas of Switzerland 1:25,000, Map 136.

Caduff R, Schlunegger F, Kos A, Wiesmann A (2015) A review of terrestrial radar interferometry for measuring surface change in the geosciences. Earth Surface Processes and Landforms, 40(2): 208-228.

Casagli N, Catani F, Del Ventisette C, Luzi G (2010) Monitoring, prediction, and early warning using ground-based radar interferometry. Landslides, 7(3): 291-301.

Crosetto M, Monserrat O, Luzi G, Cuevas-Gonzalez M, Devanthery N (2014) A noninterferometric procedure for deformation measurement using GB-SAR imagery. IEEE Geoscience and Remote Sensing Letters, 11(1): 34-38.

Crosta, G B, Di Prisco C, Frattini P, Frigerio G, Castellanza R, Agliardi F (2014) Chasing a complete understanding of the triggering mechanisms of a large rapidly evolving rockslide. Landslides, 11(5): 747-764.

Fukuzono T (1985) A new method for predicting the failure time of a slope. Proceedings of the 4th International Conference and Field Workshop in Landslides, Tokyo (Japan): pp. 145-150.

Jaboyedoff M, Oppikofer T, Abellán A, Derron M H, Loye A, Metzger R, Pedrazzini A (2012) Use of LIDAR in landslide investigations: a review. Natural hazards, 61(1): 5-28.

Lowry B, Gomez F, Zhou W, Mooney M A, Held B, Grasmick J (2013) High resolution displacement monitoring of a slow velocity landslide using ground based radar interferometry. Engineering Geology, 166: 160-169.

Metternicht G, Hurni L, Gogu R (2005) Remote sensing of landslides: An analysis of the potential contribution to geo-spatial systems for hazard assessment in mountainous environments. Remote sensing of Environment, 98(2): 284-303.

Scambos T A, Dutkiewicz M J, Wilson J C, Bindschadler R A (1992) Application of image cross-correlation to the measurement of glacier velocity using satellite image data. Remote Sensing of Environment, 42(3): 177-186.

Strozzi T, Luckman A, Murray T, Wegmüller U, and Werner C L (2002) Glacier motion estimation using SAR offset-tracking procedures, IEEE Transactions on Geoscience and Remote Sensing, 40(11): 2384–2391.

Strozzi T, Werner C, Wiesmann A, Wegmüller U (2012) Topography mapping with a portable real-aperture radar interferometer. IEEE Geoscience and Remote Sensing Letters, 9(2): 277-281.

Tarchi D, Casagli N, Moretti S, Leva D, Sieber A J (2003) Monitoring landslide displacements by using ground-based synthetic aperture radar interferometry: Application to the Ruinon landslide in the Italian Alps. Journal of Geophysical Research: Solid Earth, 108(B8).

Werner C, Wiesmann A, Strozzi T, Kos A, Caduff R, Wegmüller U (2012) The GPRI multi-mode differential interferometric radar for ground-based observations. Proceedings of 9th European Conference on Synthetic Aperture Radar, EUSAR, 23-26 April 2012. Nuremberg, Germany, pp. 304-307.

Wood J L, Harrison S, Turkington T A R, Reinhardt L (2016) Landslides and synoptic weather trends in the European Alps. Climatic Change, 136(2), 297-308.

Caduff Rafael (✉)

GAMMA Remote Sensing, Worbstrasse 225, CH-3073 Gümligen, Switzerland

E-mail: caduff@gamma-rs.ch

Strozzi Tazio

GAMMA Remote Sensing, Worbstrasse 225, CH-3073 Gümligen, Switzerland

E-mail: strozzi@gamma-rs.ch